Numerical characterization of symmetry properties for photonic crystals with hexagonal lattice

Carlo Barth[a], Jürgen Probst[a], Sven Herrmann[b], Martin Hammerschmidt[b], and Christiane Becker[a]

[a]Helmholtz-Zentrum Berlin für Materialien und Energie, Kekuléstr. 5, 12489 Berlin, Germany
[b]Zuse Institute Berlin, Takustr. 7, 14195 Berlin, Germany

ABSTRACT

We present a numerical method to characterize the symmetry properties of photonic crystal (PhC) modes based on field distributions, which themselves can be obtained numerically. These properties can be used to forecast specific features of the optical response of such systems, e.g. which modes are allowed to couple to external radiation fields. We use 2D PhCs with a hexagonal lattice of holes in dielectric as an example and apply our technique to reproduce results from analytical considerations. Further, the method is extended to fully vectorial problems in view of 3D PhCs and PhC slabs, its functionality is demonstrated using test cases and, finally, we provide an efficient implementation. The technique can thus readily be applied to output data of all band structure computation methods or even be embedded – gaining additional information about the mode symmetry.

Keywords: Photonic crystals, Point group, Photonic band structure, Leaky modes

1. INTRODUCTION

Specific modes in photonic crystal (PhC) slabs couple to the external light field and can generate largely enhanced electromagnetic fields close to the PhC surface.[1,2] These so-called leaky modes can be excited from external sources and may thus be used to influence the fluorescence properties of surface-near emitters such as quantum dots[3] or molecules.[4] Band structure computations provide not only resonance frequencies but also additional information about the spatial distribution of enhanced fields and symmetry properties. When trying to understand the optical response of PhCs by means of the photonic band structure, the symmetry of the eigenmodes cannot be neglected. E.g. for PhC slabs with 2D symmetry, modes exist which cannot be excited by external plane waves although they lie above the so-called light cone.[5,6] This restriction is only caused by a mismatch of symmetry[7] and it is thus not sufficient to calculate the photonic band structure in view of the mode frequencies and polarizations. Moreover, if the contrast in the refractive indices of the involved materials is large, it is not possible to estimate the mode frequencies from comparison to a plane-wave case or an averaged slab, making a numerical characterization of the symmetry properties indispensable. This is because perturbation theory is no longer applicable in such cases and the frequency order of the modes can change. However, the type of symmetry and hence the way in which the characterization has to be carried out strongly depends on the system geometry and can in consequence not be generalized. For this reason, automatic symmetry characterization is not implemented in any of the widely used band structure computation tools.

In this study we develop a numerical technique for automatic symmetry characterization which can easily be adapted to different system geometries and actually apply it to the case of hexagonal lattice PhCs. We give a brief synopsis of the mathematics and physics involved for this special case and show that the method gives accurate results for scalar and vectorial problems. Finally, we list our efficient implementation using the Python-language.

Further author information: (Send correspondence to Carlo Barth)
Carlo Barth: E-mail: carlo.barth@helmholtz-berlin.de, Telephone: +49 30 8062 - 41360

2. THEORY AND METHODS

2.1 Symmetry operations and point groups

From the wide field of group theory, we only consider a very limited part and may restrict mathematical rigor for simplicity. A *point group* $\mathcal{P}$, for our purposes, is a set of symmetry operations R_i

$$\mathcal{P} = \{R_0, R_1, \ldots, R_n\}, \quad n \in \mathbb{N}, \tag{1}$$

which has a group structure with composition as group operation, i.e. is closed under composition. The composition is associative and each operation has an inverse. We denote the group operations multiplicatively. Each operation R can be represented by an orthogonal matrix which we denote by $\tilde{R}$. PhCs are systems with a spatially periodic permittivity $\epsilon(\mathbf{r})$. This periodicity causes the system to be invariant under certain symmetry operations and the totality of these operations determines its point group. Conventional notations of these groups and their properties can be found in appropriate text books.[8,9]

A point of great importance is the action of a symmetry operation R on *scalar* fields $f\colon S \to \mathbb{R}$ for $S \subseteq \mathbb{R}^n$ and *vector* fields $\mathbf{F}\colon S \to \mathbb{R}^n$ for $S \subseteq \mathbb{R}^n$. We can evaluate the action of R on a scalar field by evaluating the field on the spatial coordinates transformed by the inverse operation as expressed by the following commutative diagrams.

$$\begin{array}{ccc} S & \xrightarrow{\tilde{R}} & S \\ & \searrow^{f} & \downarrow{\scriptstyle Rf} \\ & & \mathbb{R} \end{array} \qquad Rf(\mathbf{r}) = f\left(\tilde{R}^{-1}\mathbf{r}\right). \tag{2}$$

In contrast, the action of R on a vector field can be evaluated by

$$\begin{array}{ccc} S & \xrightarrow{\tilde{R}} & S \\ {\scriptstyle \mathbf{F}}\downarrow & & \downarrow{\scriptstyle R\mathbf{F}} \\ \mathbb{R}^n & \xrightarrow{\tilde{R}} & \mathbb{R}^n \end{array} \qquad R\mathbf{F}(\mathbf{r}) = \tilde{R}\mathbf{F}\left(\tilde{R}^{-1}\mathbf{r}\right), \tag{3}$$

i.e. by evaluating the vector field on the inversely transformed spatial coordinates and subsequently transforming the resulting field vector. These general considerations will be of importance when implementing the technique in later sections.

2.2 Symmetry of photonic crystals with hexagonal lattices

2.2.1 The C_{6v} point group

From now on, we restrict our study to 2D PhCs and PhC slabs with a hexagonal lattice of holes. A 2D PhC is defined as a dielectric material which is periodic in the xy-plane and with infinite extension to the direction normal to the lattice plane, i.e. the z-direction. A PhC slab is a dielectric membrane which is periodic in the xy-plane and thin in z-direction and may also have a substrate and/or superstrate. The Brillouin zone of such systems is shown in Fig. 1(a). The dielectric constant of all of the mentioned systems exhibits at least the symmetry of the C_{6v} point group, described by the symmetry operations

$$C_{6v} = \{E, C_6, C_6^{-1}, C_3, C_3^{-1}, C_2, \sigma_x, \sigma_x', \sigma_x'', \sigma_y, \sigma_y', \sigma_y''\}. \tag{4}$$

Here, E is the identity operation, while operations named C_n^m denote rotations of $2\pi m/n$ around the origin, and operations named $\sigma_{x/y}$ denote mirror reflections on the x/y-planes (and conjugate reflections). All rotations and reflections are illustrated in Fig. 1(b) by the blue and red operations, respectively. Some of these operations are conjugate, i.e. they are interchangeable by transforming the coordinate system by valid symmetry operations. These redundant operations (semi-transparent in Fig. 1(b)) do not need to be considered and we can rewrite Eq. (4) as

$$C_{6v} = \{E, 2C_6, 2C_3, C_2, 3\sigma_x, 3\sigma_y\}, \tag{5}$$

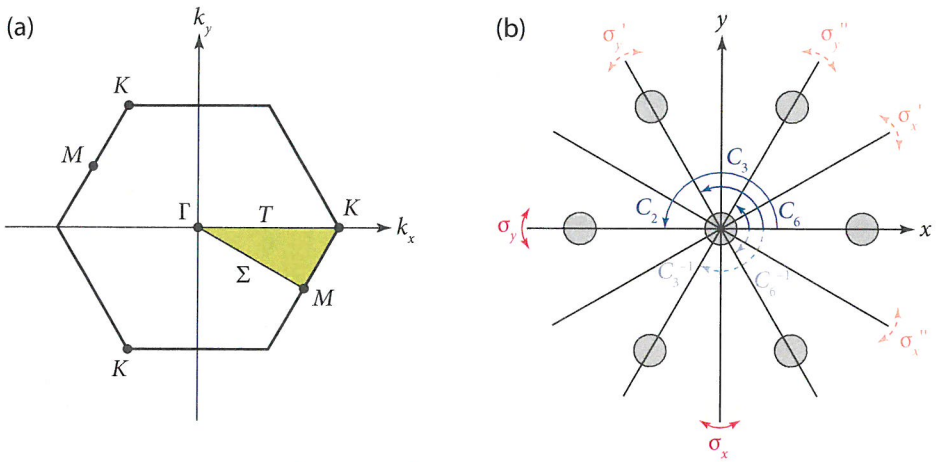

Figure 1: Symmetry properties of the hexagonal lattice (freely adapted from[7]). (**a**) First Brillouin zone and irreducible Brillouin zone (green) with high symmetry points Γ, M, and K, as well as named intermediate points T and Σ (all points on each of the segments). (**b**) Symmetry operations. Rotations are shown in blue, while mirror flips are shown in red. Operations which are conjugate to other operations appear semi-transparent and with dashed lines.

where the factor in front of the operations marks the number of conjugate operations in the corresponding class. In case of a photonic crystal slab with cylindrical holes and identical substrate and superstrate, e.g. surrounded by air, we find an even higher symmetry because of the mirror symmetry regarding the xy-plane. The point group is called D_{6h}, which is the direct product $C_{6v} \times C_{1h}$ and will not be covered in more detail.

2.2.2 Characters χ and irreducible representations $\mathcal{I}$

The photonic band structure of a PhC is the totality of all solutions $\mathbf{E}_{\mathbf{k},n}$ or $\mathbf{H}_{\mathbf{k},n}$ of the Maxwell equations for the system with the band index n and the wave vector $\mathbf{k}$. The wave vector can be regarded as the position inside the irreducible Brillouin zone and the photonic band structure is usually solved along the outline of this zone, i.e. along the connections between the high symmetry points marked in Fig. 1(a). Each solution is a so-called *irreducible representation* $\mathcal{I}$ of its point group $\mathcal{P}_\mathbf{k}$ and we list the point groups for the specific wave vectors here

$$\begin{aligned}
\mathcal{P}_\Gamma &= C_{6v}, \\
\mathcal{P}_K &= \{E, 2C_3, 3\sigma_y\} = C_{3v}, \\
\mathcal{P}_M &= \{E, C_2, \sigma_y'', \sigma_x''\} = C_{2v}, \\
\mathcal{P}_T &= \{E, \sigma_y\} = C_{1h}, \\
\mathcal{P}_\Sigma &= \{E, \sigma_x''\} = C_{1h}.
\end{aligned} \tag{6}$$

The point of the highest symmetry is thus the Γ-point, exhibiting the same symmetry as the system itself. The C_{6v} point group exhibits six irreducible representations, labeled A_1, A_2, B_1, B_2, E_1 and E_2. These are the eigenfunctions of the symmetry operations R, which themselves commute with the operators that describe the physical system.[7,10] Hence, any eigenfunction $\mathbf{E}_{\mathbf{k},n}$ or $\mathbf{H}_{\mathbf{k},n}$ of the Maxwell equations itself should be attributed to one of these irreducible representations. The spatial symmetry of an irreducible representation is expressed by its *character* χ respective a symmetry operation R, which is defined by

$$R f_\mathcal{I}(\mathbf{r}) = \chi_\mathcal{I}(R) f_\mathcal{I}(\mathbf{r}), \tag{7}$$

for an irreducible representation $f_\mathcal{I}$, in the scalar case. A similar relation applies for the vectorial case.[7] The characters of the irreducible representations for the C_{6v} point group are listed in Tab. 1. In group theory, the irreducible representations are usually given in an appropriate (in general non-Cartesian) basis, which has

Table 1: Character table of the C_{6v} point group.

$\mathbf{C_{6v}}$	**E**	$\mathbf{2C_6(z)}$	$\mathbf{2C_3(z)}$	$\mathbf{C_2(z)}$	$\mathbf{3\sigma_y}$	$\mathbf{3\sigma_x}$
$\mathbf{A_1}$	+1	+1	+1	+1	+1	+1
$\mathbf{A_2}$	+1	+1	+1	+1	−1	−1
$\mathbf{B_1}$	+1	−1	+1	−1	+1	−1
$\mathbf{B_2}$	+1	−1	+1	−1	−1	+1
$\mathbf{E_1}$	+2	+1	−1	−2	0	0
$\mathbf{E_2}$	+2	−1	−1	+2	0	0

the advantage that the dimensionality of the transformation matrices is irreducible. In this basis, the absolute values of the characters are direct implications of the matrix-dimensionality. The A- and B-representations are one-dimensional, while the E-representations are two-dimensional and can thus also take values of ± 2.

2.2.3 Degenerate modes

A special case occurs for degenerate modes, i.e. modes with identical frequency and polarization. The point groups which are of interest for hexagonal PhCs (Eq. (6)) only exhibit irreducible representations labeled by A, B and E. Non-degenerate modes are always of A- or B-type, while degenerate modes are of E-type – a consequence of their matrix-dimensionality as stated above. When considered independently, the field solutions of the degenerate modes do not necessarily exhibit a valid symmetry of the corresponding point group. However, any linear combination of degenerate eigenfunctions is an eigenfunction as well and a linear combination exists which corresponds to an irreducible representation. In our case, this linear combination is always of E-type.

2.3 Numerical calculation of characters χ for the C_{6v} point group

2.3.1 General algorithm

To numerically determine the irreducible representation $f_{\mathcal{I}}$ of a mode, the characters χ_i for all symmetry operations R_i of the point group need to be calculated. The irreducible representation is then given from comparison with Tab. 1. We need to distinguish the 2D (scalar) and the 3D (vectorial) cases. When dealing with 2D problems, we only look at a single component of the electric or magnetic field, respectively, since the Maxwell equations decouple into two independent sets for TE and TM polarization.[11] These are scalar fields $f(\mathbf{r})$ and can be treated by Eq. (2). With 3D PhCs and PhC slabs, we deal with the complete vectorial field since a decoupling of the Maxwell equations is no longer present, i.e. using Eq. (3).

In the 2D case, we solve the photonic band structure for the TE and TM polarizations separately. It is sufficient to consider the z-component of the magnetic field for TE, and the electric field for TM, respectively. Since the calculation is carried out for a 2D geometry, we end with a field of dimensionality $N_x \times N_y$, where N is the number of points in the respective direction. In the 3D case, all components of either the E- or the H-field need to be considered and we have a 3D-space, resulting in a field of dimensionality $N_x \times N_y \times N_z \times 3$. For the hexagonal lattice the computational domain is usually a hexagon in 2D and a prism with a hexagonal base in 3D. It is crucial that we consider the field only in this space for our numerical approach. If the field export is on a rectangular grid, the data needs to be restricted to the computational domain. The algorithm can then be described by the following steps.

1. Set up an interpolator for each of the necessary components of the field $\mathbf{F}$ to be able to evaluate it at any spatial coordinate inside the computational domain.
2. For each of the symmetry operations R_i, calculate transformed coordinates $\mathbf{r}_t$ by applying the inverse of the transformation matrix $\tilde{R}_i^{-1}$ to the initial coordinates.
3. Evaluate the field $\mathbf{F}$ at the new coordinates $\mathbf{r}_t$ using the interpolator(s), yielding $\mathbf{F}_{i,t}$.
4. Only in the 3D-case: apply the transformation matrix to the field, i.e. calculate $\tilde{R}_i \mathbf{F}_{i,t}$.)

5. Calculate the normalized covariance matrix C^{norm} of the initial and the transformed fields to find the characters $\chi(R_i)$.

Detailed explanations for the important steps will be given in the next sections. We list here the 3D matrices $\tilde{R}$ which correspond to the operations of the C_{6v} point group. In the 2D case, the last column and row are omitted.

$$\tilde{C}_n^m = \begin{pmatrix} \cos(2\pi m/n) & -\sin(2\pi m/n) & 0 \\ \sin(2\pi m/n) & \cos(2\pi m/n) & 0 \\ 0 & 0 & 1 \end{pmatrix}, \qquad \tilde{\sigma}_{y/x} = \begin{pmatrix} \pm 1 & 0 & 0 \\ 0 & \mp 1 & 0 \\ 0 & 0 & 1 \end{pmatrix} \tag{8}$$

2.3.2 Evaluation of field values

The evaluation of field values necessitated by Eqs. (2) and (3) can enforce to calculate field values on spatial coordinates which are not included in the initial field, in the general case. For that reason, we included the interpolation step in the general algorithm. However, for some of the transformations, e.g. mirror reflections and rotations by multiples of 90°, there are no such new coordinates and an interpolation is unnecessary. If an appropriate basis is chosen for the simulation it can even be completely omitted. That way, the algorithm can be optimized to a great extent for specific geometries.

However, to keep the algorithm general we will no longer concentrate on these kinds of optimizations and use the interpolation method instead. The interpolation routine influences the accuracy of the solution, but also the computational costs. There is a trade-off with the number of exported field values N, since a larger N gives a higher accuracy but slows down the evaluation of the interpolator significantly. Using a nearest-neighbor interpolation is fast, but can give slightly worse results for transformations which introduce new spatial coordinates, as stated above. See Sec. 3.2 for more details and a convergence study.

2.3.3 Calculation of characters χ using covariance

As can be seen from Eq. 7, the characters χ can be determined by comparing the initial and the transformed fields, which can be done using the normalized covariance matrix C^{norm}. Efficient implementations of this method are present in most programming languages, including MATLAB and Python. The entries C_{ij}^{norm} of the normalized covariance matrix, which are also known as the Pearson product-moment correlation coefficients,[12] state the linear correlation between two variables and can take values between $+1$ and -1. It is thus useful to identify if a field is identical to its transformed field ($C_{01}^{\text{norm}} = C_{10}^{\text{norm}} \approx +1$) or if it is flipped ($C_{01}^{\text{norm}} = C_{10}^{\text{norm}} \approx -1$). Degenerate modes do note exhibit all symmetries in general, so that values in between can occur. We will show that these values are suitable for the calculation of the actual character as well in Sec. 3.1. We note that the correlation matrix is not independent of the choice of conjugate mirror operations, but it will be shown as well that it is non-relevant for the resulting character in the end.

3. RESULTS

3.1 Scalar case: characters of modes on the Γ-point of 2D hexagonal PhCs

To demonstrate our approach for the scalar case we calculated the characters for a 2D PhC with hexagonal lattice at the Γ point. The system is described in chapter 3 of the book *Optical Properties of Photonic Crystals* by K. Sakoda,[7] where the characters are also examined by analytical considerations and are used here as a reference. The radius of the air holes is $r = 0.42a$ with lattice constant a and the relative permittivity of the dielectric is $\epsilon_r = 2.72$. We used the open-source software package MIT Photonic-Bands (MPB[13]) to calculate the lowest 8 bands with a resolution of 1024 for the TE and TM polarization, respectively. Depending on the polarization, we exported the H- or E-field on a rectangular grid of size 256×222 for each band. When restricting the points to those lying inside the hexagon, there are 42392 of the initial 56832 points left for the analysis. We further used a linear interpolation routine for the evaluation of the fields on transformed coordinates. These parameters assure a minimal relative deviation as will be shown in Sec. 3.2.

Figures 4 and 5 on pages 311 and 312 show the results of the initial field (column 1) for each band (rows) inside the hexagonal area and the numerically transformed fields for all of the five non-trivial transformations

(columns 2–6) of the C_{6v} point group. The resonance frequency ω in dimensionless units is shown in each title of column 1, while the calculated normalized covariance is shown in the title of the columns of the transformed fields. We omit the indication of a color scale since the images use individual scales and absolute field values are not of interest for the study.

For both polarizations, the lowest band corresponds to the trivial solution of either polarization. Especially for the TM-case, the E_z component is close to zero and causes problems in the calculation of the correlation matrix. We work around this by returning a correlation of $+1$ if all field values are close to zero in the implementation. These solutions hence correspond to the irreducible representation A_1. For higher bands the algorithm works as expected as can be seen by eye when looking at the field patterns.

For the degenerate modes, which can be identified by their almost matching frequency, one does not find characters that can be matched to an irreducible representation with Tab. 1 at first glance. This is because for degenerate bands their linear combinations are also eigenfunctions, but in general neither of them alone shows a particular symmetry (see Sec. 2.2.3). We obtain the correct characters by adding the calculated correlation coefficients for each of the degenerate couples. We attribute this behavior to the fact that the character χ is the trace of the transformation matrix of the 2D basis of the E-representation noted in Sec. 2.2, although further research is necessary to verify this assumption.

The complete results for the determination of the irreducible representations are listed in Tab. 2. For the TE-polarization in Tab. 2(a), we find an A_1 and a B_2 mode as the energetically lowest solutions, followed by a doubly degenerate E_1 and a doubly degenerate E_2. The next two solutions are both of A_1-type again. Similar conclusions apply to the TM-case listed in Tab. 2(b). The order of irreducible representations exactly matches the ones provided in the reference.[7]

Table 2: Calculated characters χ and irreducible representations (column irr. rep.) for the 2D PhC with $r = 0.42a$ and $\epsilon_r = 2.72$ at the Γ-point.

(a) TE-polarization

$\omega a/2\pi c$	$2C_6$	$2C_3$	C_2	$3\sigma_y$	$3\sigma_x$	irr. rep.
0.00000	1	1	1	1	1	A_1
0.91018	−1	1	−1	−1	1	B_2
0.92392	1	−1	−2	0	0	E_1
0.92421	1	−1	−2	0	0	E_1
0.96004	−1	−1	2	0	0	E_2
0.96024	−1	−1	2	0	0	E_2
1.04902	1	1	1	1	1	A_1
1.48156	1	1	1	1	1	A_1

(b) TM-polarization

$\omega a/2\pi c$	$2C_6$	$2C_3$	C_2	$3\sigma_y$	$3\sigma_x$	irr. rep.
0.00000	1	1	1	1	1	A_1
0.75677	−1	1	−1	−1	1	B_2
0.83807	−1	−1	2	0	0	E_2
0.83829	−1	−1	2	0	0	E_2
0.98460	1	1	1	1	1	A_1
1.04620	1	−1	−2	0	0	E_1
1.04648	1	−1	−2	0	0	E_1
1.38643	1	1	1	1	1	A_1

3.2 Convergence in relation to MPB resolution and interpolation routine

We study the convergence of our approach by calculating the normalized covariance for two different modes in relation to the MPB resolution r_{MPB}. When increasing r_{MPB} the convergence of the MPB simulation improves itself quadratically[13] and further the number of points of the output field increases – which both may affect the convergence of the character calculation. We calculated the relative deviation from the expected character for band 2 of the TE-polarization and band 5 of the TM-polarization when rotating around $\pi/3$ and π, respectively (see. Figs. 4 and 5). The results are shown in Fig. 2, both for linear (blue, solid) and nearest-neighbor interpolation (green, dashed). We observe that for both interpolation methods the convergence is roughly proportional to the square of the MPB resolution (note the doubly logarithmic scale), i.e. identical to the convergence of MPB itself. For a rotation of π, this rule is almost satisfied exactly and linear interpolation does not give any advantage because the rotated spatial coordinates coincide with known coordinates. For an angle of $\pi/3$ the linear interpolation gives slightly better results, but anyway increasing the MPB resolution has a much stronger

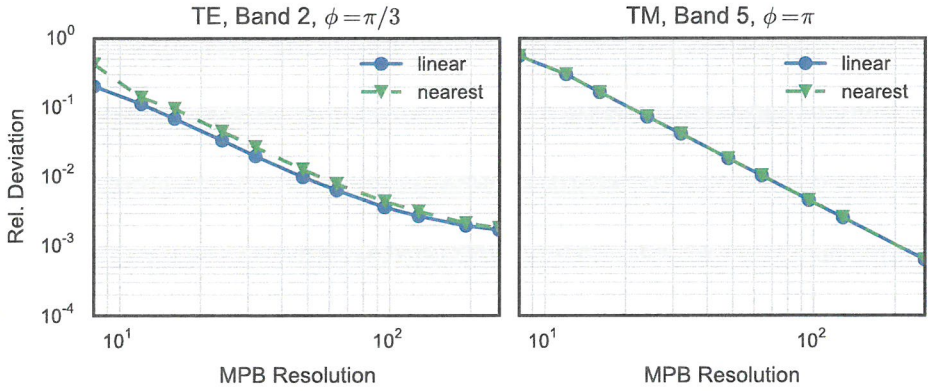

Figure 2: Relative deviation for the character calculation of two different modes as a function of MPB resolution and interpolation method (doubly logarithmic scale). (**left**) A mode with character of -1 for a rotation of $\pi/3$. (**right**) A more trivial mode with character of $+1$ for a rotation of π.

effect. The interpolation seems to limit the accuracy for angles which are not multiples of $\pi/2$ since we observe a saturation effect in the left panel which is not present in the right one.

3.3 Vectorial case: characters of a test case field

The vectorial case is a generalization of the scalar case and is treated almost in the same way. We need three interpolation steps – one for each component – and we need to transform the field itself after the evaluation as described in Sec. 2.3. For easier visualization we demonstrate the process on a 2D test vector field, defined by

$$\mathbf{F}(x,y) = \begin{pmatrix} 1 \\ |y| \end{pmatrix}. \tag{9}$$

The results for the numerical transformations of the C_{6v} point group are shown in Fig. 3. The field direction, marked by arrows, is transformed as expected. The calculated correlations are provided in the title of each image in columns 2–6. We observe that this particular field exhibits only the C_2 symmetry, with a character of -1.

4. DISCUSSION AND CONCLUSION

The presented algorithm was able to reproduce the analytical reference results at the Γ point using numerical calculations in the 2D case. The extension to the vectorial case was demonstrated in brief using a test case. Degenerate modes have been treated by adding the normalized covariances of each involved mode and we gained the correct irreducible representations this way. Using the compatibility relations from group theory, we can even forecast the symmetry of the bands at the Σ and T points from these results without any additional numerical effort.[7] For example, we know that a B_2 mode at the Γ point is transformed into a B mode when moving into K-direction, but into an A mode when moving into M-direction. This is of great importance, since in contrast to an A mode a B mode can not be excited by an external plane wave.[14] Hence, this knowledge is indispensable for the design of optical systems based on the photonic band structure if an interaction with external plane waves is intended. This additional information can also be of use for band structure calculations as a verification of the provided solutions. E.g. if spurious modes can be returned by the technique these could be identified by their inconsistent symmetry properties. Also, when trying to trace a single band, its symmetry properties can be used to distinguish it from different bands. In this case, the compatibility relations need to be considered as well.

We presented an all-numerical technique for the assignment of PhC modes to irreducible representations of the corresponding point group. The technique exhibits no limitations in view of the applicability to different PhC geometries. It can readily be applied to the results of any numerical band structure solver and hence give additional information about the symmetry properties of photonic bands. This information can be of great

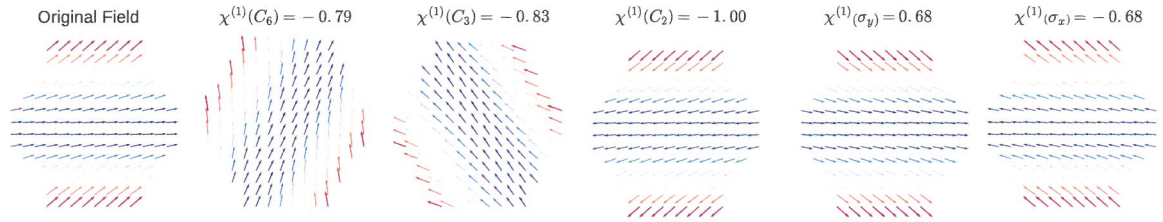

Figure 3: Numerical field transformations of a test vector field. For each of the transformations of the C_{6v} point group the transformed field is shown in columns 2–6, marked with the calculated correlation.

importance for the optical properties of each band, for example when studying transmission through a PhC or the coupling of modes to external radiation fields.[5,6] In contrast to analytical considerations, there is no limitation for the dielectric contrast or the frequency of the modes of interest. It may thus be of great value for the characterization of complex systems such as 3D PhCs or PhC slabs with additional substrates and large dielectric contrasts.

APPENDIX A. IMPLEMENTATION IN PYTHON

We list a minimal implementation of the algorithm using the Python-language for the 2D case. It can be applied using the `transformField`-function if the field, the coordinates and the transformation matrices are available as NumPy-arrays using the call

```
fieldMasked, transformedFields = transformField(coords, field, transMatrices)
```

The correlation can then be calculated by

```
compareFields(fieldMasked, transformedFields[i])
```

for each transformed field i.

Listing 1: Minimal implementation of the algorithm for the symmetry characterization of modes (scalar case). The function `transformField` is used to calculate the necessary transformations of the input field. The correlation can then be calculated using the `compareFields`-function.

```
# Import of modules
import numpy as np
import pandas as pd
from scipy import interpolate

def isInsideHexagon(x, y, d=2., x0=0., y0=0.):
    """
    Returns the indices of the coordinates that lie inside
    a hexagon of width d centered at (x0, y0).
    """
    dx = np.abs(x - x0)/d
    dy = np.abs(y - y0)/d
    a = 0.25 * np.sqrt(3.0)
    return np.logical_not(np.logical_and(dy <= a, a*dx + 0.25*dy <= 0.5*a))

def interpolateField(points, values, method = 'linear'):
    """
    Returns an interpolator object using the specified method.
    """
    if method == 'nearest':
        return interpolate.NearestNDInterpolator(points, values)
    elif method == 'linear':
```

```
        return interpolate.LinearNDInterpolator(points, values)

def applyTransformation(matrix, coordsFlat, interp, originalShape):
    """
    Applies a transformation using the given transformation matrix
    to the given coordinates using the interpolator object. The
    result is reshaped to the given originalShape.
    """
    matrix_inv = np.linalg.inv(matrix) # inverse transformation matrix

    # transform the cartesian coordinates unsing the inverse matrix
    coordsNew = matrix_inv.dot(np.ma.MaskedArray(coordsFlat))

    # evaluate the field components on the new coordinates
    fieldAtModCoords = interp(np.array(coordsNew).T)

    # tansform the new field using the original transformation matrix
    Ftrans = fieldAtModCoords.T.reshape(originalShape)
    return Ftrans

def transformField(coords, field, transformationMatrices,
                   interpMethod='nearest'):
    """
    Applies all transformations given by the transformationMatrices
    to the field with the given coordinates. The field is restricted
    to the hexagonal area using a masked array. Returns the masked
    initial fields and all transformed fields.
    """
    # store the original shape
    shape = field.shape

    # Restrict points to those lying inside an hexagon using
    # numpy's masked arrays
    idxInHex = isInsideHexagon(coords[0], coords[1])
    coordsMasked = [np.ma.masked_where(idxInHex, c) for c in coords]
    fieldMasked = np.ma.masked_where(idxInHex, field)
    fieldmask_ = fieldMasked.mask # store the original mask

    # Flatten the coordinates and the field and set up the interpolator
    coordsFlat = [c.ravel() for c in coordsMasked]
    fieldFlat = fieldMasked.ravel()
    interp = interpolateField(np.ma.MaskedArray(coordsFlat).T,
                              fieldFlat,
                              method=interpMethod)

    # Perform all transformations and store the resulting fields
    transformedFields = []
    for tm in transformationMatrices:
        Ftrans = applyTransformation(tm, coordsFlat, interp, shape)
        # apply the original mask to the field
        Ftrans = np.ma.masked_array(Ftrans, mask=fieldmask_)
        transformedFields.append(Ftrans)

    return fieldMasked, transformedFields

def compareFields(originalField, transformedField):
    """
```

```
    Calculates the normalized covariance of two fields.
    """
    if np.isclose(originalField.compressed(), 0.).all():
        # if all field values are close to zero, 1 is returned
        return 1.
    # a pandas DataFrame is constructed from the flattened
    # input fields
    df = pd.DataFrame({'in': originalField.ravel(),
                       'out':transformedField.ravel()})
    # the element (0,1) of the covariance matrix is returned
    return df.corr().iat[0,1]
```

ACKNOWLEDGMENTS

We thank Prof. Kazuaki Sakoda of the National Institute for Materials Science, Japan, for spending a lot of time on an extensive and very helpful e-mail correspondence. The German Federal Ministry of Education and Research is acknowledged for funding the research activities of the Nano-SIPPE group within the program NanoMatFutur (No. 03X5520). Further we acknowledge support by the Einstein Foundation Berlin through ECMath within subprojects SE6 and OT5. Parts of the results were obtained at the Berlin Joint Lab for Optical Simulations for Energy Research (BerOSE) of Helmholtz-Zentrum Berlin für Materialien und Energie, Zuse Institute Berlin and Freie Universität Berlin.

REFERENCES

[1] John, S., "Strong localization of photons in certain disordered dielectric superlattices," *Phys. Rev. Lett.* **58**(23), 2486–2489 (1987).

[2] Soljačić, M. and Joannopoulos, J. D., "Enhancement of nonlinear effects using photonic crystals," *Nat. Mater.* **3**(4), 211–219 (2004).

[3] Ganesh, N., Zhang, W., Mathias, P. C., Chow, E., Soares, J. a. N. T., Malyarchuk, V., Smith, A. D., and Cunningham, B. T., "Enhanced fluorescence emission from quantum dots on a photonic crystal surface.," *Nat. Nanotechnol.* **2**, 515–20 (aug 2007).

[4] Langguth, L., Punj, D., Wenger, J., and Koenderink, A. F., "Plasmonic Band Structure Controls Single-Molecule Fluorescence," *ACS Nano* **7**, 8840–8848 (oct 2013).

[5] Robertson, W. M., Arjavalingam, G., Meade, R., Brommer, K., Rappe, a., and Joannopoulos, J., "Measurement of photonic band structure in a two-dimensional periodic dielectric array," *Phys. Rev. Lett.* **68**(13), 2023–2026 (1992).

[6] Robertson, W. M., Arjavalingam, G., Meade, R. D., Brommer, K. D., Rappe, A. M., and Joannopoulos, J. D., "Measurement of the photon dispersion relation in two-dimensional ordered dielectric arrays," *J. Opt. Soc. Am. B* **10**, 322 (feb 1993).

[7] Sakoda, K., [*Optical Properties of Photonic Crystals*], vol. 80 of *Springer Series in Optical Sciences*, Springer-Verlag, Berlin/Heidelberg (2005).

[8] Cornwell, J. F., [*Group theory and electronic energy bands in solids*], John Wiley International Publishers, New York (1969).

[9] Inui, T., Tanabe, Y., and Onodera, Y., [*Group theory and its applications in physics*], Springer, Berlin (1990).

[10] Joannopoulos, J. D., Johnson, S. G., Winn, J. N., and Meade, R. D., [*Photonic crystals: molding the flow of light*], Princeton University Press, 2. ed. (2008).

[11] Jackson, J. D., [*Classical Electrodynamics*], John Wiley & Sons, New York, 3. ed. (sep 1999).

[12] Pearson, K., "Note on Regression and Inheritance in the Case of Two Parents," *Proc. R. Soc. London* **58**, 240–242 (jan 1895).

[13] Johnson, S. G. and Joannopoulos, J. D., "Block-iterative frequency-domain methods for Maxwell's equations in a planewave basis," *Opt. Express* **8**(3), 363–376 (2001).

[14] Ochiai, T. and Sakoda, K., "Dispersion relation and optical transmittance of a hexagonal photonic crystal slab," *Phys. Rev. B* **63**, 125107 (mar 2001).

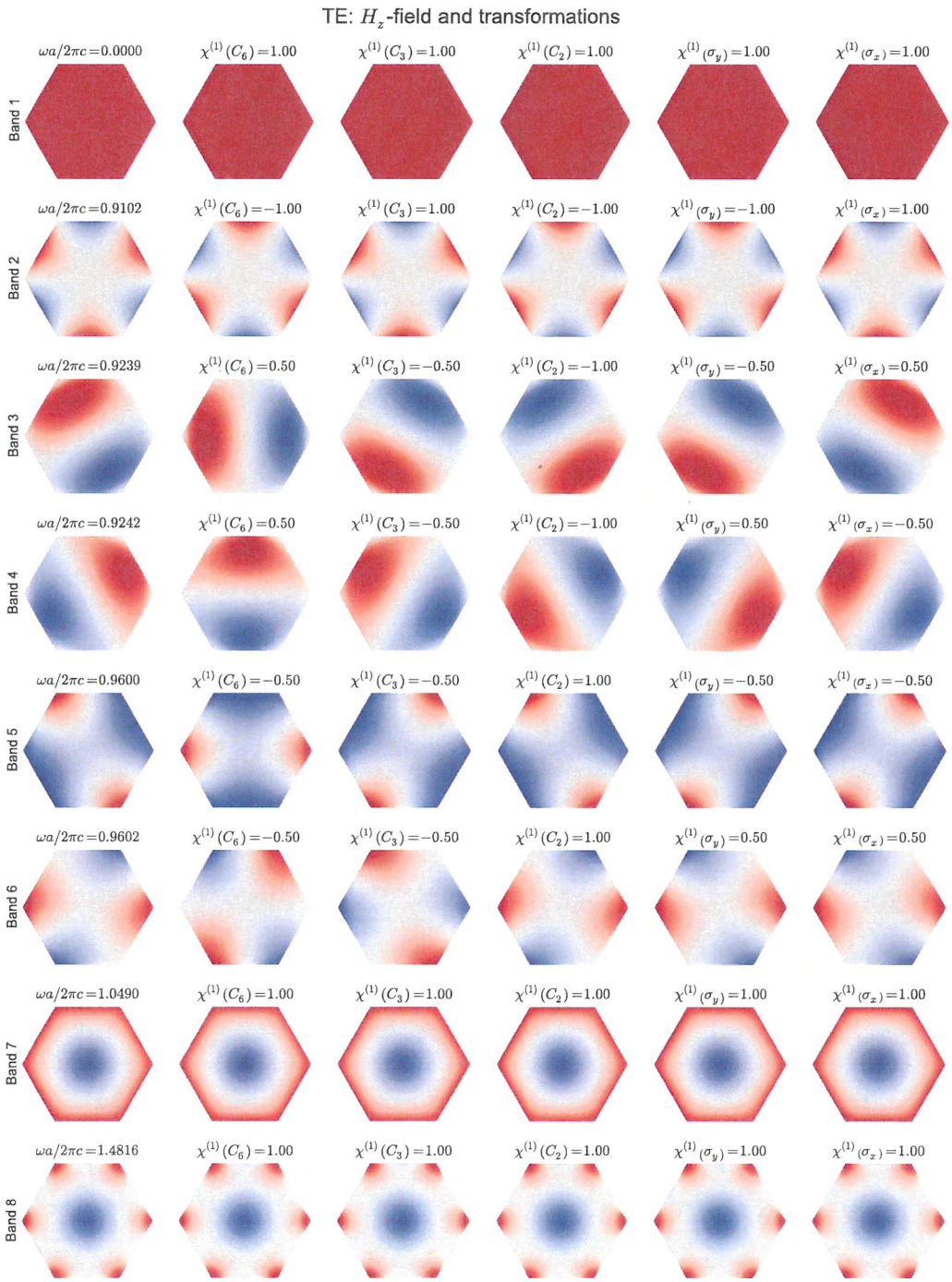

Figure 4: Numerical field transformations for the TE-polarization. The initial field derived from an MPB simulation is shown in column 1, marked with band index and resonance frequency ω in dimensionless units. The field is restricted to the hexagonal area, i.e. a unit cell. Numerically transformed fields for all of the five transformations (columns 2–6) of the C_{6v} point group, marked with the calculated normalized covariance.

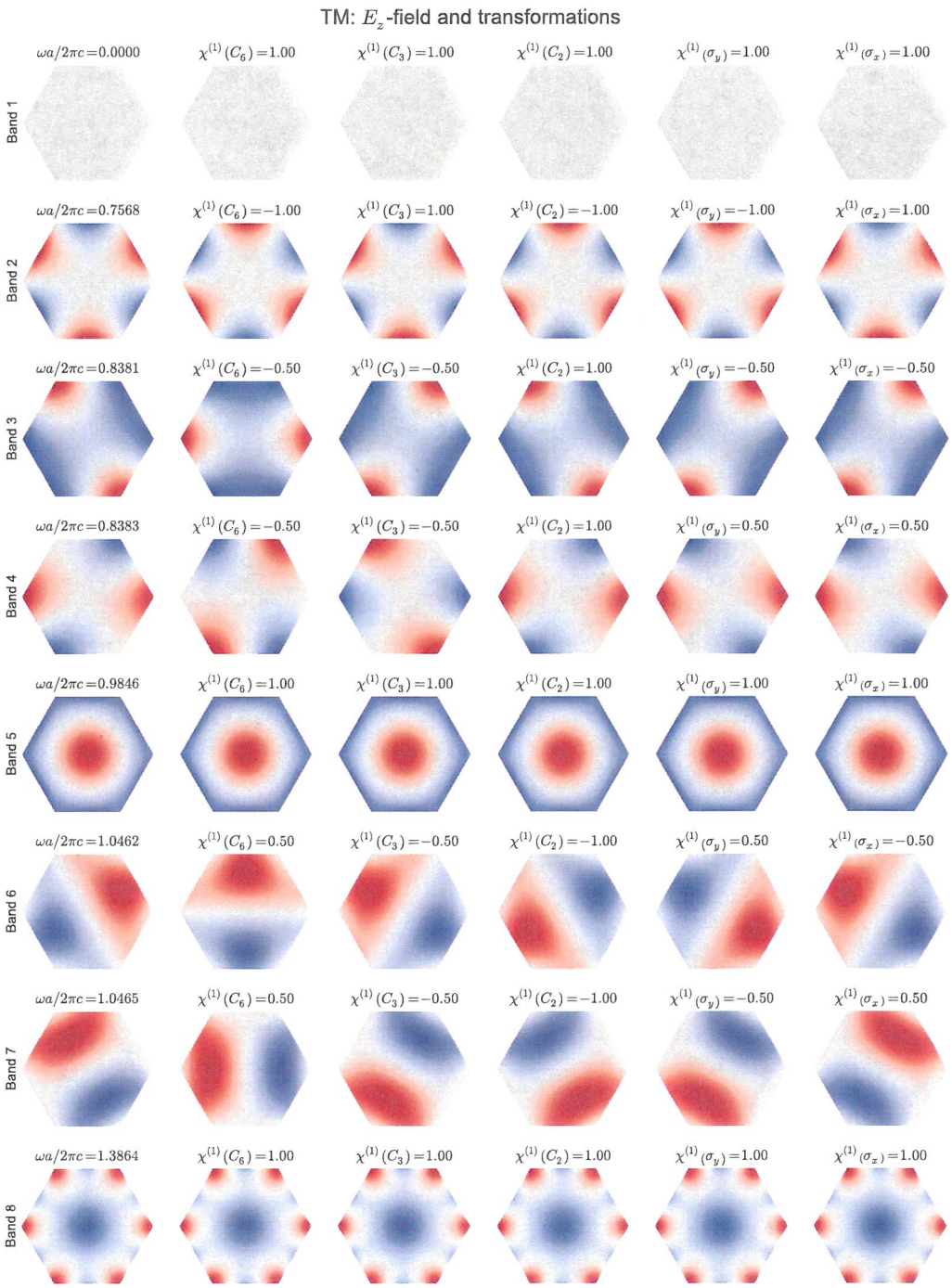

Figure 5: Numerical field transformations for the TM-polarization. The initial field derived from an MPB simulation is shown in column 1, marked with band index and resonance frequency ω in dimensionless units. The field is restricted to the hexagonal area, i.e. a unit cell. Numerically transformed fields for all of the five transformations (columns 2–6) of the C_{6v} point group, marked with the calculated normalized covariance.